PHYSICAL REVIEW A **83**, 020302(R) (2011)

Surface code quantum computing with error rates over 1%

David S. Wang, Austin G. Fowler, and Lloyd C. L. Hollenberg
Centre for Quantum Computation and Communication Technology, School of Physics, The University of Melbourne, Victoria 3010, Australia
(Received 20 September 2010; published 18 February 2011)

Large-scale quantum computation will only be achieved if experimentally implementable quantum error correction procedures are devised that can tolerate experimentally achievable error rates. We describe an improved decoding algorithm for the Kitaev surface code, which requires only a two-dimensional square lattice of qubits that can interact with their nearest neighbors, that raises the tolerable quantum gate error rate to over 1%. The precise maximum tolerable error rate depends on the error model, and we calculate values in the range 1.1–1.4% for various physically reasonable models. These values represent a very high threshold error rate calculated in a constrained setting.

DOI: 10.1103/PhysRevA.83.020302 PACS number(s): 03.67.Pp, 05.50.+q

Building a quantum computer is a daunting task. Engineering the ability to interact nonlocal pairs of qubits is particularly challenging. All existing quantum error correction (QEC) schemes capable of tolerating error rates above 1% assume the ability to deterministically interact pairs of qubits separated by arbitrary distances with no time or error rate penalty [1–3]. The most recent of these works estimates a threshold error rate p_{th} of 5% [3].

It is far more physically reasonable to assume a two-dimensional (2D) lattice of qubits with only nearest neighbor interactions, proposed realizations of which exist for ion traps [4], optical lattices [5], superconducting qubits [6], optically addressed quantum dots [7,8], nitrogen-vacancy (N-V) centers in diamond [9], and many other systems. For such proposals, the leading QEC scheme [10,11], which is based on the Kitaev surface code [12,13], has been shown to possess a p_{th} of 0.75% [10,14,15]. We increase this to 1.1–1.4%, depending on the error model, and substantially improve the high error rate performance, resulting in a fivefold reduction of the required number of qubits at an operating error rate of 0.5%. We achieve this by carefully using the given error model to calculate approximate probabilities of different error events, and not initializing qubits. Note that related 3D topological cluster state work exists [16–18], and the techniques we describe could be used to improve the threshold of these schemes as well, however we focus on the surface code here.

To overview, we begin by describing stabilizers and our simplified quantum gate sequence, followed by a detailed discussion of how probable different error events are and how this information can be fed into the classical decoding algorithm. We then present the results of detailed simulations, which apply two-qubit depolarizing noise with probability p_2 after two-qubit quantum gates and single-qubit depolarizing noise with probability p_I after identity gates, and which use measurement gates that report and project into the wrong eigenstate with probability p_M. In addition to the standard error model with $p_2 = p_I = p_M = p$, we simulate a balanced error model with $p_I = 4p_2/5$ and $p_M = 2p_I/3$, ensuring idle qubits have the same probability of error as a single qubit involved in a two-qubit gate and taking into account the fact that measurement is only sensitive to errors in one basis. We also simulate $p_I = p_2/1000$ and $p_M = p_2/100$, modeling typical error ratios in an ion trap.

A stabilizer [19] of a state $|\Psi\rangle$ is an operator S such that $S|\Psi\rangle = |\Psi\rangle$. Provided a method of measuring the stabilizer is available, an error E that anticommutes with S can be detected as $SE|\Psi\rangle = -ES|\Psi\rangle = -E|\Psi\rangle$. Examples of surface code stabilizers [12] are shown in Fig. 1(a). Circuits measuring these stabilizers without explicit initialization gates are shown in Fig. 2. We assume quantum nondemolition measurements, which have been experimentally demonstrated using ion traps [20], optical lattices [21], superconducting qubits [22], and N-V centers in diamond [23] and theoretically proposed for optically addressed quantum dots [24,25]. The initial and final measurements match when $+1$ is measured and differ when -1 is measured. An appropriate sequence of two-qubit gates for measuring all stabilizers across the lattice simultaneously is shown in Fig. 1(b). Data qubits execute identity gates while the syndrome qubits are measured.

Repeatedly executing Fig. 1(b) and appropriate syndrome qubit measurements and data qubit identity gates generates points in space and time where measurements change sign, indicating local errors. Renormalization techniques exist capable of processing perfect syndrome information [26,27]; however, at present only the minimum weight perfect matching algorithm [28,29] can be used to process the output of realistic quantum circuits.

The minimum weight perfect matching algorithm takes coordinates and a measure of separation and matches pairs of coordinates such that the total separation is a minimum. Chains of corrective operations connecting matched pairs can then be applied; however, in practice one would simply update the classical Pauli frame [1] to avoid introducing further errors. Prior work has calculated the separation of two syndrome changes, $s_1 = (i_1, j_1, t_1)$ and $s_2 = (i_2, j_2, t_2)$, using $d(s_1, s_2) = |i_1 - i_2| + |j_1 - j_2| + |t_1 - t_2|$ [10,14,15]; however it was shown in [30] that this is far from optimal and leads to poor performance at low error rates. In this work, we focus on the high error rate performance, and in contrast to [30], which assumed that all equal length error chains were equally probable, we approximate the probability $P(s_1, s_2)$ of a given pair of syndrome changes being connected by an error chain, and we set $d(s_1, s_2) = -\ln[P(s_1, s_2)]$. This choice of $d(s_1, s_2)$ works well as high probability pairs have low separation and are preferentially matched by the algorithm. This accounts for the substantial high error rate performance increase we observe.

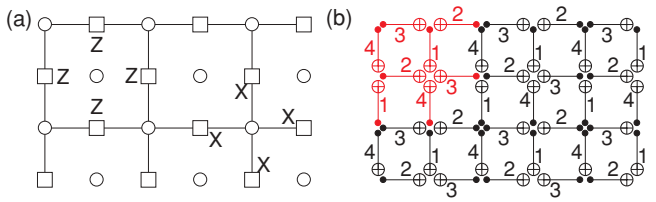

FIG. 1. (Color online) (a) Two-dimensional lattice of data qubits (squares) and syndrome qubits (circles) and examples of the data qubit stabilizers. (b) Sequence of CNOT gates permitting simultaneous measurement of all stabilizers. Numbers indicate the relative timing of gates. The highlighted gates can be tiled to fill the plane.

To calculate $P(s_1,s_2)$, we study the effect of gate errors. Figure 3 shows all possible pairs of syndrome changes resulting from all errors on all meaningfully distinct gates. The controlled-NOT gates (CNOTs) shown measure an X stabilizer. The effect of errors on the CNOT gates used to measure a Z stabilizer can be obtained by interchanging X and Z. Note that X and Z errors are corrected independently, so only tensor products of one type of error need be considered.

Working through a specific case, consider error process 6 in Fig. 3(b), a ZZ error after a CNOT gate between an ancilla (control) and a data qubit (target). The Z error on the ancilla will be detected at the completion of the current syndrome extraction cycle. The Z error on the data qubit will be copied to the ancilla to its left by the next interaction between that pair, which occurs in the same round [see Fig. 1(b)]. This double detection is represented by the horizontal line. Since X and Z errors are corrected independently, ZZ is really shorthand for ZZ, ZY, YZ, or YY.

Using Fig. 3, Fig. 4 was constructed, grouping gate errors leading to specific geometrically separated pairs of syndrome changes. Again working through a specific case, a vertical pair of changes [Fig. 4(a)] can arise from error processes 1, 7, 11, 18, and 21 from Fig. 3. Error process 21 is a measurement error and therefore has probability p_M. As discussed above, the others each correspond to 4 of the 15 possible tensor product errors. Explicitly, error process 1 (ZI) corresponds to ZI, ZX, YI, and YX and therefore has probability $4p_2/15$. Error processes 7, 11, and 18 similarly each have probability $4p_2/15$. The probability of an odd number of error processes occurring in each group gives the probability of the presence of the associated link. Using the standard error model, the probability of the vertical link shown in Fig. 4(a) is

$$p_A = \frac{16p}{15}\left(1-\frac{4p}{15}\right)^3(1-p)+p\left(1-\frac{4p}{15}\right)^4+O(p^3). \tag{1}$$

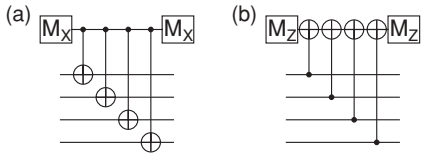

FIG. 2. Circuits determining the sign of a stabilizer (a) $S = XXXX$ or (b) $S = ZZZZ$ without explicit initialization gates.

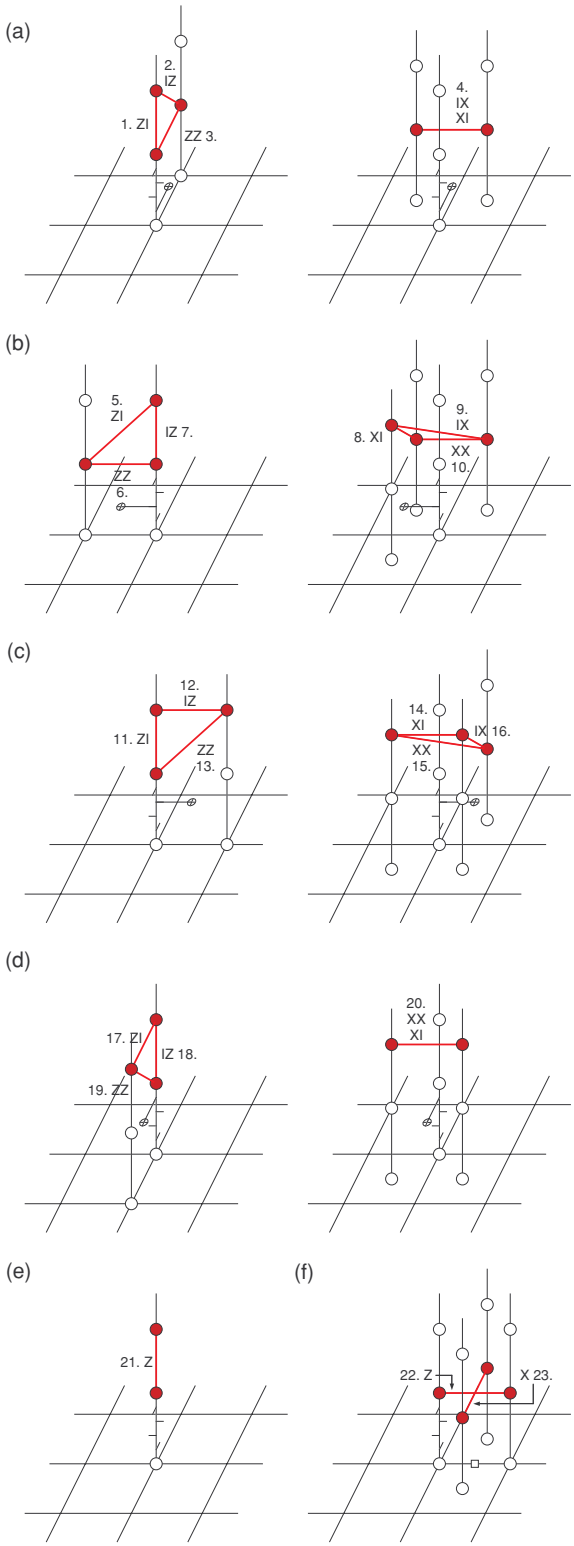

FIG. 3. (Color online) Observed syndrome changes as a result of a single error. The vertical axis is time, the horizontal grid represents Fig. 1(a), and only relevant qubit world lines are shown. A CNOT gate suffering an error is drawn in full; otherwise it is represented by a tick mark protruding in the direction of application. Syndrome changes occur in pairs. Pairs of changes (shaded circles connected by lines) resulting from (a–d) specific two-qubit errors on specific CNOT gates, (e) a syndrome qubit measurement error, and (f) a data qubit memory error.

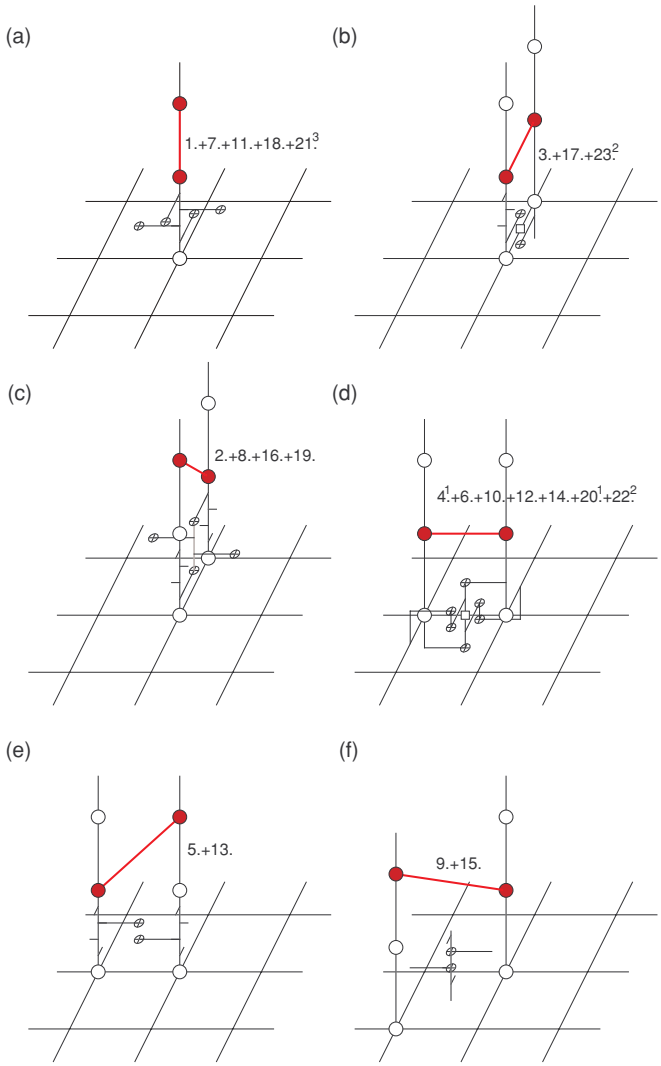

FIG. 4. (Color online) Numbered error processes from Fig. 3 contributing to specific links. Superscripts 1, 2, and 3 indicate error processes occurring with probability $8p_2/15$, $2p_1/3$, and p_M, respectively. All others occur with probability $4p_2/15$.

Similar polynomial probability expressions p_B, p_C, p_D, p_E, and p_F can be constructed for Figs. 4(b)–4(f). Some straightforward modifications of the links and expressions are required at the temporal and spatial boundaries to account for missing gates.

The probability $P(s_1,s_2)$ that two syndrome changes are connected is the sum of the probabilities of all connecting paths. The probability of a given path is the product of the link probabilities along the path, assuming independent errors. Several approximations of $P(s_1,s_2)$ are worthy of study. The simplest approximation is to take a single path of maximum probability $P_{\max}(s_1,s_2)$ and define $d_{\max}(s_1,s_2) = -\ln[P_{\max}(s_1,s_2)]$. We shall see that this approximation is sufficient to substantially increase p_{th} and that more accurate approximations do not lead to further increase. The performance of surface code QEC subjected to X errors when using $d_{\max}(s_1,s_2)$ and the standard error model is shown in Fig. 5. We obtained almost identical results for Z errors (not shown),

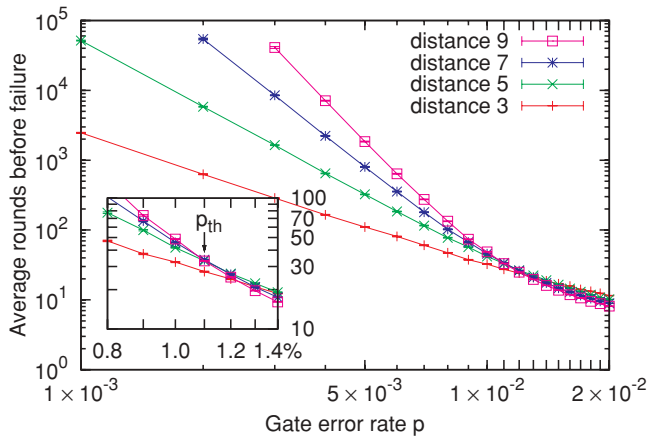

FIG. 5. (Color online) Average number of rounds of error correction before logical X failure as a function of the gate error rate p when using $d_{\max}(s_1,s_2)$ and the standard error model.

with small differences due to the lack of geometric symmetry of the link probabilities.

Figure 5 gives strong evidence of $p_{\text{th}} = 1.1\%$. We have verified this by simulating high distance codes at $p = 1.1\%$ and observing neither increase nor decrease of the failure time. This is enormously encouraging and motivates one to better approximate $P(s_1,s_2)$ in an effort to further increase p_{th}. Additional accuracy can be achieved by taking all the shortest length paths (measured in links) between s_1 and s_2 and calculating the sum of products of link probabilities along each path. We define the resulting distance measure as $d_0(s_1,s_2)$. We can define similar distance measures $d_n(s_1,s_2)$, taking into account all minimum length l paths and paths of length no greater than $l+n$. The performance of surface code QEC around p_{th} using $d_0(s_1,s_2)$ is shown in Fig. 6. It can be seen that p_{th} remains 1.1%.

The fact that d_0 leads to the same p_{th} as using a single maximum probability path distance measure $d_{\max}$ can be explained by noting that $d_0(s_1,s_2)$ only differs from $d_{\max}(s_1,s_2)$ if s_1 and s_2 are separated by at least two links. Single-link paths are

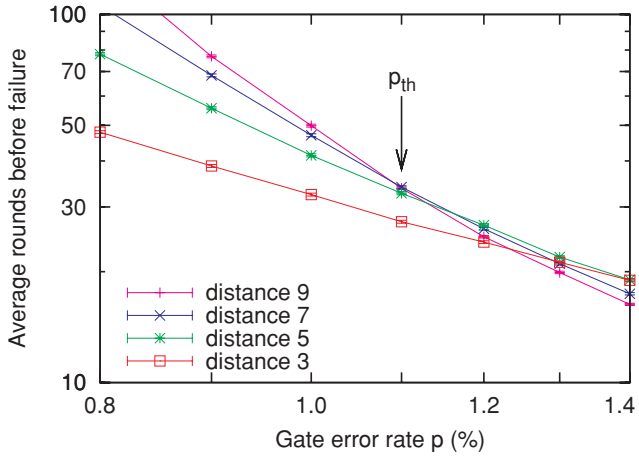

FIG. 6. (Color online) Average number of rounds of error correction before logical X failure as a function of the gate error rate p when using $d_0(s_1,s_2)$ and the standard error model. The threshold error rate p_{th} remains 1.1%.

unique minimum length paths implying $d_0 = d_{\max}$. The vast majority of error chains, even for $p = p_{\text{th}}$, are only single-link chains, as the threshold error rate is well below the percolation threshold. We find the distance modification resulting from taking into account the multiple paths connecting syndrome changes separated by multiple links is of order 10–20%. Given that multiple-link paths are not leading order contributors to p_{th} in the first place, this relatively small weight change does not result in an observable improvement of p_{th}.

Higher-order approximations $d_n(s_1,s_2)$ will also result in the same p_{th} as the distance measure is hardly altered by increasing n. A typical example of $p = 0.01$, $s_1 = (0,0,0)$, and $s_2 = (1,-1,0)$ gives $d_0 = 6.91$ (6 paths), $d_1 = 6.86$ (30 paths), and $d_2 = 6.85$ (390 paths). The exponential increase of the number of paths is well balanced by the exponential decrease of their probability.

The balanced error model is a better model of all quantum gates failing with equal probability than the standard error model, and appropriate modification of the polynomials using $p_2 = p$, $p_I = 4p/5$, and $p_M = 8p/15$ leads to $p_{\text{th}} = 1.2\%$. The ion trap error model, with $p_2 = p$, $p_I = p/1000$, and $p_M = p/100$ leads to $p_{\text{th}} = 1.4\%$. Arbitrary stochastic error models are straightforward to analyze using our formalism.

To conclude, by performing a detailed study of the probability of different pairs of syndrome changes and feeding the simplest approximation of this information into the minimum weight perfect matching algorithm, we have been able to raise the geometrically constrained threshold error rate to 1.1–1.4%, depending on the exact error model, while maintaining computational efficiency. There is the potential for still further improvement by taking into account correlations between X and Z errors.

The practical significance of the threshold increase can be appreciated by noting that our scheme requires five times fewer qubits than the previous best surface code scheme [30] to achieve a given logical error rate at $p = 0.5\%$, with only a distance 23 code required to extend the lifetime of a qubit by a factor of 10^5. Alternatively, [30] requires $p = 8 \times 10^{-4}$ for the logical error rate to decrease by an order of magnitude when the distance of the code is increased by 2, whereas from Fig. 5 it can be seen that our scheme can do the same at $p = 2 \times 10^{-3}$. These substantial relaxations of the experimental requirements arise purely from better classical processing.

This research was conducted by the Australian Research Council Centre of Excellence for Quantum Computation and Communication Technology (Project No. CE110001029) with support from the US National Security Agency and the US Army Research Office under Contract No. W911NF-08-1-0527.

[1] E. Knill, Nature (London) **434**, 39 (2005).
[2] K. Fujii and K. Yamamoto, Phys. Rev. A **81**, 042324 (2010).
[3] K. Fujii and K. Yamamoto, Phys. Rev. A **82**, 060301(R) (2010).
[4] R. Stock and D. F. V. James, Phys. Rev. Lett. **102**, 170501 (2009).
[5] D. Jaksch, Contemp. Phys. **45**, 367 (2004).
[6] D. P. DiVincenzo, Phys. Scr. T **137**, 014020 (2009).
[7] R. VanMeter, T. D. Ladd, A. G. Fowler, and Y. Yamamoto, Int. J. Quantum Inf. **8**, 295 (2010).
[8] N. C. Jones, R. VanMeter, A. G. Fowler, P. L. McMahon, J. Kim, T. D. Ladd, and Y. Yamamoto, e-print arXiv:1010.5022.
[9] N. Y. Yao, L. Jiang, A. V. Gorshkov, Z.-X. Gong, A. Zhai, L.-M. Duan, and M. D. Lukin, Phys. Rev. Lett. **106**, 040505 (2011).
[10] R. Raussendorf and J. Harrington, Phys. Rev. Lett. **98**, 190504 (2007).
[11] R. Raussendorf, J. Harrington, and K. Goyal, New J. Phys. **9**, 199 (2007).
[12] S. B. Bravyi and A. Y. Kitaev, e-print arXiv:quant-ph/9811052.
[13] E. Dennis, A. Kitaev, A. Landahl, and J. Preskill, J. Math. Phys. **43**, 4452 (2002).
[14] A. G. Fowler, A. M. Stephens, and P. Groszkowski, Phys. Rev. A **80**, 052312 (2009).
[15] D. S. Wang, A. G. Fowler, A. M. Stephens, and L. C. L. Hollenberg, Quantum Inf. Comput. **10**, 456 (2010).
[16] D. A. Herrera-Martí, A. G. Fowler, D. Jennings, and T. Rudolph, Phys. Rev. A **82**, 032332 (2010).
[17] S. D. Barrett and T. M. Stace, Phys. Rev. Lett. **105**, 200502 (2010).
[18] Y. Li, S. D. Barrett, T. M. Stace, and S. C. Benjamin, e-print arXiv:1008.1369.
[19] D. Gottesman, Ph.D. thesis, Caltech, e-print arXiv:quant-ph/9705052.
[20] A. H. Burrell, D. J. Szwer, S. C. Webster, and D. M. Lucas, Phys. Rev. A **81**, 040302(R) (2010).
[21] J. Kruse, C. Gierl, M. Schlosser, and G. Birkl, Phys. Rev. A **81**, 060308(R) (2010).
[22] A. Lupascu, E. F. C. Driessen, L. Roschier, C. J. P. M. Harmans, and J. E. Mooij, Phys. Rev. Lett. **96**, 127003 (2006).
[23] F. Jelezko, T. Gaebel, I. Popa, M. Domhan, A. Gruber, and J. Wrachtrup, Phys. Rev. Lett. **93**, 130501 (2004).
[24] J. Berezovsky, M. H. Mikkelsen, O. Gywat, N. G. Stoltz, L. A. Coldren, and D. D. Awschalom, Science **314**, 1916 (2006).
[25] M. Atatüre, J. Dreiser, A. Badolato, and A. Imamoglu, Nature. Phys. **3**, 101 (2007).
[26] G. Duclos-Cianci and D. Poulin, Phys. Rev. Lett. **104**, 050504 (2010).
[27] G. Duclos-Cianci and D. Poulin, e-print arXiv:1006.1362.
[28] J. Edmonds, Canad. J. Math. **17**, 449 (1965).
[29] J. Edmonds, J. Res. Natl. Bur. Standards **69B**, 125 (1965).
[30] A. G. Fowler, D. S. Wang, and L. C. L. Hollenberg, Quantum Inf. Comput. **11**, 8 (2011).